Icarus **144**, 397–409 (2000)
doi:10.1006/icar.1999.6301, available online at http://www.idealibrary.com on IDEAL®

Variability of Mars' North Polar Water Ice Cap

II. Analysis of Viking IRTM and MAWD Data

Deborah S. Bass

Instrumentation and Space Research Division, Southwest Research Institute, P.O. Drawer 28510, San Antonio, Texas 78228-0510
E-mail: dsb@grouse.space.swri.edu

and

David A. Paige

Department of Earth and Space Sciences, University of California, Los Angeles, 405 Hilgard Avenue, Los Angeles, California 90095-1567

Received May 15, 1998; revised June 10, 1999

We have examined Viking Orbiter albedo, thermal, and atmospheric water vapor data acquired during Mars' northern summer season and compared these results with the imaging results of D. S. Bass, K. E. Herkenhoff, and D. A. Paige (2000, *Icarus* 144, 382–396). The Viking thermal mapper data show an increase in the albedo of the entire north water ice cap, consistent with imaging data results. We find a strong correlation between polar cap surface temperature and atmospheric water vapor, but we note that the atmospheric water vapor data do not increase dramatically until the cap center temperature exceeds 200 K. The Viking Infrared Thermal Mapper data support the conclusion that cold trapping is the correct explanation for the observed late summer brightening of the residual water ice cap. We suggest that the retreating seasonal carbon dioxide cap takes the water with it and not until the receding cold trap reaches the cap center is the bulk of the water released into the atmosphere. This process, plus the deposition of fresh ice onto the cap later in the summer season, will tend to close the north polar cap's annual water cycle.

Key Words: **Mars; Mars, surface; Mars, atmosphere; Mars, climate; surfaces, planets.**

1. INTRODUCTION

The visible appearance of the martian residual north polar cap and its seasonal/interannual variability has been examined in Bass *et al.* (2000) which hereafter will be described as Part I. That paper points out that certain regions of the north residual water ice cap grow brighter later in the summer season and that the phenomenon may be explained by the deposition of water ice onto the cap. Part I also investigates the minimum amount of potentially deposited ice mixed with Mars dust that could have produced the late summer brightening. Here we examine the observations of the thermal infrared appearance, albedo (surface brightness), and atmospheric water vapor content of the north polar region in light of the hypothesis of water ice deposition in the summer season. We also use the implications of these results to investigate the potential implications for the global and seasonal water cycles. Because the polar caps are potentially large sources and sinks of the volatiles involved in climate dynamics, examining changes in the polar cap appearance is a key to understanding climate change on Mars.

1.1. Spacecraft Observations of Mars

Others have described the Viking Infrared Thermal Mapper (IRTM) and Viking Mars Atmospheric Water Detector (MAWD) instruments and data in detail (e.g., Kieffer 1976, Davies *et al.* 1977). Briefly, the IRTM and MAWD instruments were included in both Viking Orbiter payloads. IRTM and MAWD observations spanned all phases of the Viking mission. IRTM was a 28-channel, four-telescope radiometer that operated in six spectral bands. Each of the four telescopes had 7 channels, with footprints arranged in a chevron pattern. The spectral bands measured radiation in bands centered at 7, 9, 11, 15, and 20 μm, as well as a 0.3- to 3-μm solar channel. The field of view of IRTM overlapped that of the imaging camera as well as the Mars Atmospheric Water Detector, providing directly coincident coverage (Snyder, 1979). The Viking MAWD was a 5-channel grating spectrometer that operated in the 1.4-μm region; 3 of the channels were centered on absorbing regions and 2 on the continuum between them to obtain integrated water column abundances.

IRTM and MAWD demonstrated that the northern residual cap is composed of water ice. IRTM and MAWD data showed that temperatures and albedos are consistent with CO_2 ice in the fall and winter seasons and H_2O ice in the summer (Kieffer *et al.*

0019-1035/00 $35.00

1976, 1977). MAWD observed spatial and temporal variations of water vapor at 1.4 μm. The maximum atmospheric water column abundance ($\sim$100 precipitable μm or 10^{-2} g/cm^2) occurs over Mars' northern polar region in the summer season, suggesting that the northern residual summer cap is a water source (Farmer *et al.* 1976). Davies *et al.* (1977) mapped the extent of the water vapor over the north polar cap in the spring and summer seasons. They pointed out that the maximum peak of water vapor was not over the center of the cap, as expected, but rather over the dark sand sea directly surrounding the cap.

1.2. Models of the Martian Water Cycle

The north polar cap of Mars and associated layered terrains are very important to the martian water cycle, as suggested by model results. The two-dimensional transport model of Haberle and Jakosky (1990) is one of the most complete two-dimensional models of the martian water cycle to date. Coupled to a diffusive boundary layer model, they showed that the bulk source of the southern hemispheric atmospheric water vapor is not the north polar cap but rather must be the southern regolith. In the northern hemisphere, the cap can not account for all the water vapor in the northern atmosphere so the regolith must play an important role there as well. The water that evaporates off the permanent water ice cap in the northern hemisphere is transported southward during the summer months. Haberle and Jakosky (1990) model results showed that water may be deposited at the cold south pole, in the equatorial regolith as an adsorbate, or it may be returned to the cap by baroclinic eddies that are characteristic of the fall, winter, and spring general circulation. In any case, the martian low latitudes are extremely dry, with typical relative humidities of a few percent near the surface. One important result of the Haberle and Jakosky (1990) model is the off-cap circulation present near the edge of the retreating polar cap due to the temperature differential between the cold polar ice cap and the warmer, ice-free surrounding terrains.

Houben *et al.* (1997) employ a spectral global circulation model with simplified radiation physics and a hydrological cycle coupled to a parameterized two-layer subsurface model to model the water cycle. With 32 grid points pole to pole, the model has approximately 5° of resolution. Water acts as a passive tracer in the model, and there is no cloud albedo effect; rather, the atmosphere is saturated whenever there is ice on the surface. Further, a diurnal cycle is not considered, nor is topography. An interesting result of this model is a mechanism for moving water vapor poleward as the seasonal CO_2 cap retreats in the spring (Houben *et al.* 1997). At the edges of the sublimating CO_2 ice cap, water vapor is taken into the atmosphere. Due to baroclinic wave activity at the cap edge, some of this water vapor is transported back across the still iced, colder region at which point the water vapor precipitates out back onto the cap. As the season continues, the CO_2 cap gradually decreases in size and continues to move poleward, taking the water ice with it. Finally, just after summer solstice, a large pulse of water vapor is released into the atmosphere.

At the present time, the source of the north polar water vapor, as well as its transport in and out of the polar regions, is not well constrained. Furthermore, whether or not the conditions presently observed on Mars correspond to those that existed when the bulk of the polar layered deposits were emplaced is

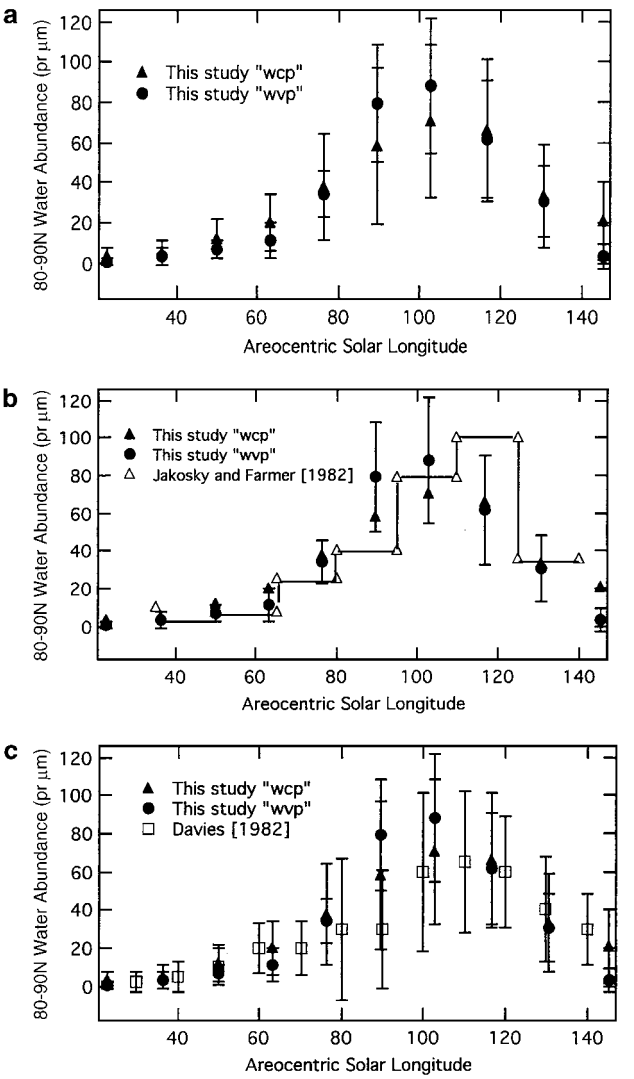

FIG. 1. MAWD seasonally and topographically varying pressure (at 200 K) integrated column atmospheric water vapor abundances, wvp data, and integrated column atmospheric water vapor abundances calculated with a constant pressure (6 mbar) and temperature (200 K), wcp data. Values were acquired for 80 to 90°N latitude bands. Values from this study are averages of data acquired in 30 Julian days. Those dates were subsequently converted to areocentric solar longitude. Error bars are $\pm$1 SD. (a) MAWD wcp data compared to the wvp data. Higher total water column abundances are reached with the wvp data than with the wcp data, but the peak occurs at approximately the same time. (b) Jakosky and Farmer (1982) values compared to wcp and wvp values computed in this study. Values were approximated from published data in Fig. 2, Jakosky and Farmer (1982). (c) Davies (1982) data compared to wcp and wvp values computed in this study. Davies (1982) values were approximated from published data, Fig. 2, Davies (1982). Peak water abundance values occur at similar areocentric solar longitude.

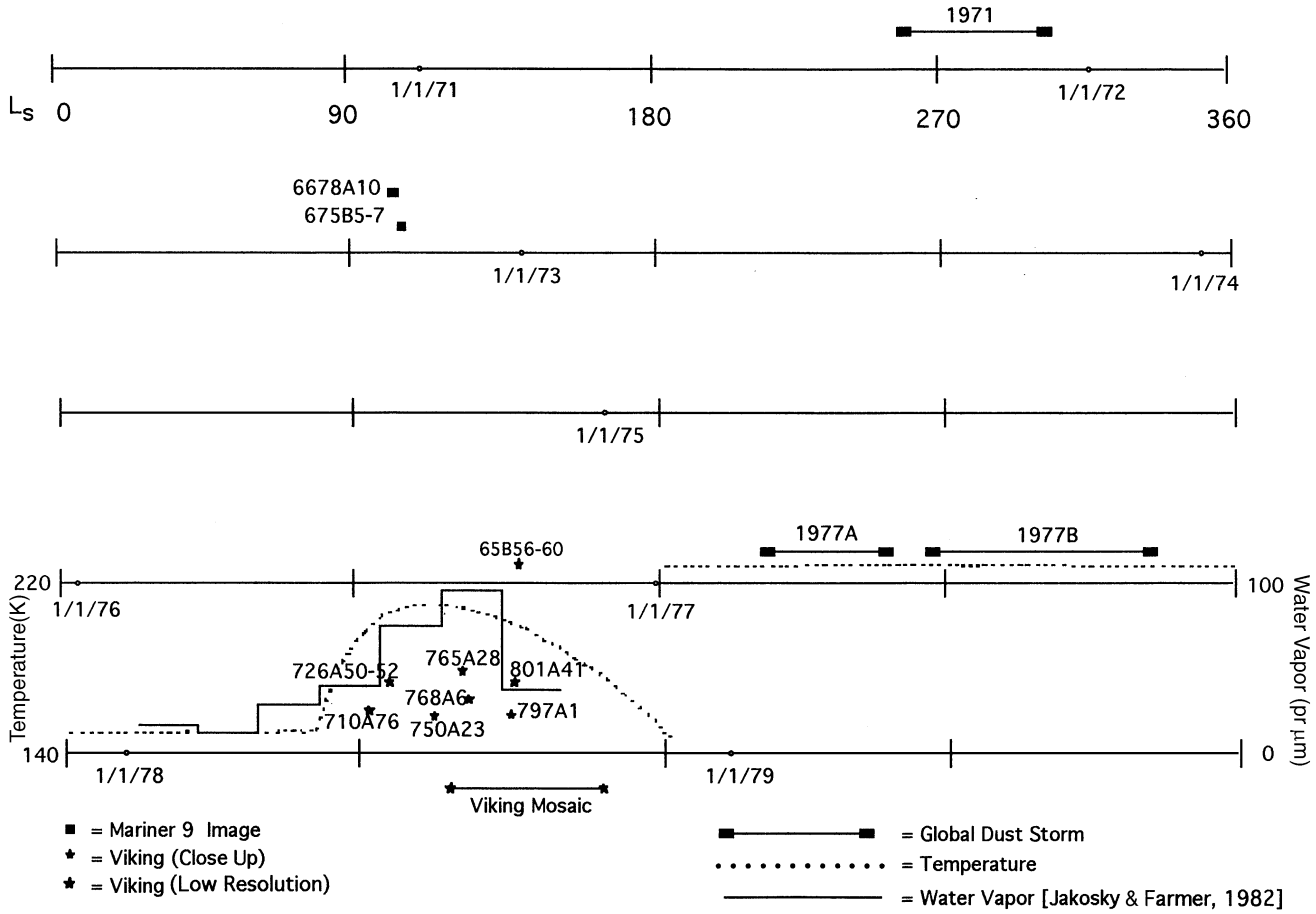

FIG. 2. Plot of areocentric solar longitudes of images included in this study as well as relevant global dust storms from Mariner 9 through Viking Orbiter missions. Sequence of images in Part I, Fig. 2, are represented by closed stars. Sequence of images in Part I, Fig. 3, are represented by open stars. North polar cap surface temperatures for 1 Mars year from Viking Orbiter IRTM observations are plotted (Paige and Ingersoll 1985) as well as atmospheric water column abundances from Viking Orbiter MAWD observations (Jakosky and Farmer 1982).

unknown, but learning the current source of water vapor, as well as the mechanisms involved in water transport, is a logical step toward defining past conditions. Understanding the present-day martian annual water cycle is required before polar laminae can be interpreted in terms of past climatic conditions on Mars.

2. VIKING INFRARED THERMAL MAPPER AND VIKING MARS ATMOSPHERIC WATER DETECTOR DATA PROCESSING

Direct comparison of Mariner 9 imaging, Viking imaging, Viking IRTM, and Viking MAWD datasets has not been attempted previously. The IRTM data selected for this analysis were published in a CD-ROM released by the NASA Planetary Data System. We selected data acquired from December 24, 1997, to September 19, 1978 (Julian date 2443501 through 2443771, $L_s = 23.69$–146.00). (L_s, or areocentric solar longitude, corresponds to season in the martian year, where $L_s = 0$ is the northern hemisphere vernal equinox, $L_s = 90$ is the northern hemisphere summer solstice, and so forth.) The dates we chose corresponded to Mars' early spring and summer seasons in the northern hemisphere, when the seasonal CO_2 cap was retreating and the residual water ice cap was exposed from 60°N–90°N. We chose to use IRTM 20-μm channel brightness temperatures (T_{20}) for surface thermal mapping, and IRTM broad-band-solar channel data which spanned the wavelength region from 0.3 to 3.0 μm for apparent albedo mapping. Observations acquired with emission angles greater than 60° were excluded, since those data were acquired through a path length of ≥ 2 airmasses.

The IRTM data were projected to polar coordinates to produce maps of the north polar region from 65°N to 90°N using square bins with averaged data from 2° of latitude and 2° of longitude. Each "map" represents the data acquired during "L_s" intervals that correspond to the number of Julian days in that number of areocentric solar longitudes. The polar maps of IRTM albedo data approximately correlate with various Viking Orbiter images from Part I. The maps only approximately correlate as there was not enough albedo data acquired during a given day to create a complete map. We also created (T_{20}) surface brightness temperature maps that correspond to both the imaging and the albedo

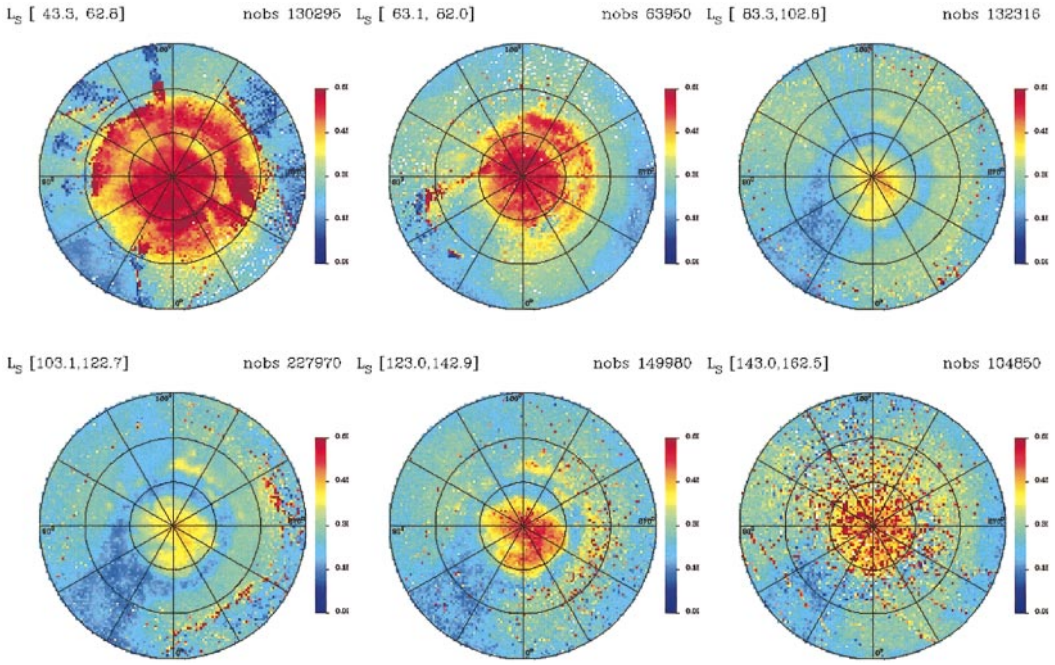

FIG. 3. Six IRTM albedo maps showing increase in brightness of northern residual water ice cap as summer season progresses. "Nobs" refers to the number of observations present in each map. Maps show data binned in increments of 40 Julian days and those dates are converted to areocentric solar longitude. Data are binned in 2° by 2° intervals. Albedos range from 0.12 (blue) to 0.60 (red). Emission angles <60°.

data to closely determine the surface temperatures and conditions on the cap when the images identified in Part I and other data were acquired.

Viking MAWD data were obtained from a magnetic tape written in 1983 in a format similar to that used for the IRTM data (Robert Mehlman, personal communication, 1996). We matched the MAWD records identified by date and time to the dates and times of IRTM data by converting MAWD IRKs (number of rasters since observation start) to IRTM ICKs, given that 1 IRK = 0.28 s, 1 ICK = 1.12 s, 1 FDS (observation sequence counter) = 4.48 s, and 1 Julian day = 86,400 s. We correlated our converted MAWD data with published sequences of IRTM data (Kieffer 1977, Davies 1982) to be certain comparisons could be made of IRTM and MAWD data acquired at the same time: the Julian dates of each MAWD observation are accurate to 10^{-4} days.

Averaged radiances of the 5 MAWD channels are used for the water vapor amounts presented here; these values correspond to those denoted by the variable "water" in the MAWD data. We directly compared IRTM T_{20}, albedo, and MAWD water data acquired during the martian spring and summer seasons. The noise in the MAWD water data was too large to allow the creation of polar water maps comparable to the IRTM albedo and T_{20} maps. Instead, graphs of the average water amount, average surface temperatures, and average albedos with respect to time were plotted. The data were binned in Julian day intervals, and then those dates were converted to equivalent areocentric solar longitudes.

Caution must be used when identifying the MAWD data examined in this manuscript. Two different integrated column abundances of water vapor were defined in the MAWD data set, one using constant atmospheric pressure (6 mbar) and temperature (200 K) (MAWD "water" data, hereafter referred to as "wcp" data) and one dependent upon model calculations of seasonally varying pressures using a topographic model and a 200 K temperature (MAWD "wfapt" data, hereafter referred to as "wvp" data). Additionally, the different water amounts also result from (1) calculating averaged radiances and then determining the water abundance (wcp data) and (2) using the radiances to determine the water abundances and then averaging (wvp data) (Richard Zurek, personal communication, 1997). Figure 1a shows MAWD wcp data compared to the wvp data from 80 to 90°N. We took the wcp and wvp values from the MAWD dataset and binned them in 30 Julian days and then converted those dates into areocentric solar longitude. Our analysis of MAWD wvp data resulted in different abundances of water vapor from the MAWD wcp data. Unless otherwise noted, wcp data were used in this study.

3. RESULTS

Comparison of the Viking MAWD data and IRTM data indicates that there is a correlation between surface temperature and atmospheric water vapor content. Figure 2 shows the 4 martian years that encompass the timescale when the Mariner 9 and Viking missions were in operation. The plot indicates the time

and duration of the two global dust storms that occurred during Viking Orbiter operations, as well as shows the time of each of the images shown in Part I, Figs. 2 and 3. Additionally, a rough approximation of IRTM and MAWD data are plotted to show the drop in atmospheric water vapor as the surface temperatures declined. As the summer continued, atmospheric water abundance increased, peaking at approximately $L_s = 120$ (Jakosky and Farmer 1982). Surface temperatures decreased in the late summer and early fall, producing the documented observations of increased bright ice coverage in Part I, Figs. 2 and 3). In the following sections, we describe and compare the IRTM albedo, IRTM brightness temperature, and MAWD water vapor data in greater detail.

3.1. Viking IRTM Albedo Data Results

Binned to show forty L_s increments of data, polar-projected albedo maps of the north residual polar cap show the retreat of the bright seasonal carbon dioxide cap, the exposure of a darker residual water ice cap, and the trend of increasing brightness of the residual water ice caps as the summer season progressed (Fig. 3). The trend is documented in the Orbiter images in Part I. Albedos representative of the residual water ice cap (bright region at 88°N, 62°W), the sand dunes surrounding the cap (dark regions at 78°N, 315°W), and the polar layered terrains (intermediate region at 83°N, 111°W) were identified (Fig. 4). This plot shows that the albedo of the bright and intermediate areas increases with increasing areocentric solar longitude, while the dark regions show no increase in albedo. Each point plotted in Fig. 4 is an average of four bin values at each location from the IRTM albedo maps in Fig. 3. The plot shows that the bright and intermediate regions became brighter while dark regions remained dark. Thus the brightening is not a photometric artifact resulting from spacecraft viewing geometry, nor could it be a result of cloud coverage; if this were the case, all areas of the cap would have increased uniformly in brightness.

Figure 5a shows IRTM albedo data for the zonally averaged latitude band 89–90°N as well as albedo data for 82–83°N, 270–330°W. The regions were selected because they allow comparison of the perpetually bright cap center and a region that changes albedo more dramatically over the course of the spring and summer. The cap is darkest between approximately $L_s = 94$ and $L_s = 103$ (Fig. 5a) and then brightens until approximately $L_s = 140$. The center of the residual north polar cap remains bright, even when the rest of the cap is relatively dark after the seasonal CO_2 cap has completely retreated (Fig. 3; Part I, Fig. 1a).

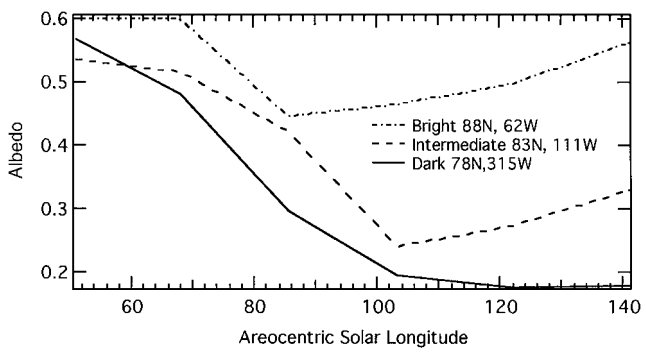

FIG. 4. Representative average albedo values for water ice (bright), polar-layered terrains (intermediate), and sand dunes (dark). Data points from the six IRTM maps (Fig. 3). Absolute albedos of bright- and intermediate-valued areas increase as northern summer season progresses. Areocentric solar longitudes correspond to the average of sequence dates plotted in Fig. 3.

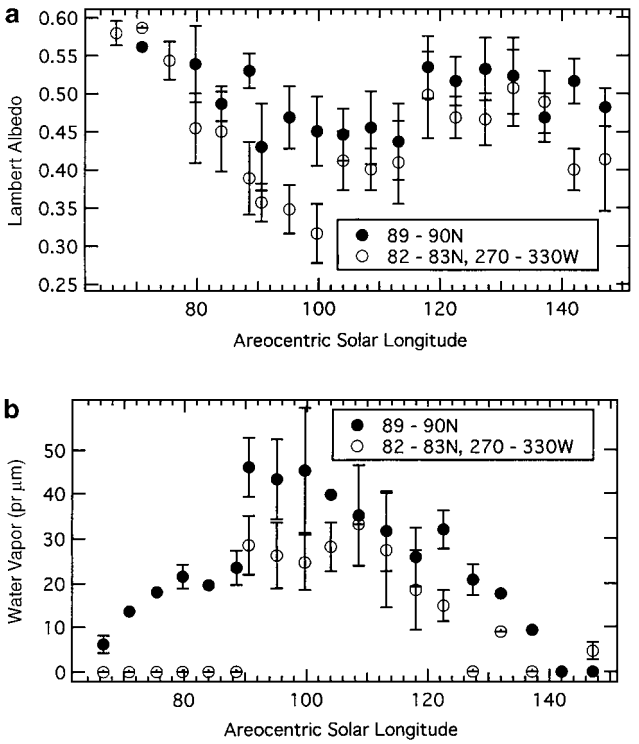

FIG. 5. IRTM albedo and MAWD water data for north residual cap center and cap edges. Values are binned in increments of 10 Julian days and those dates are converted to areocentric solar longitude. (a) IRTM albedo data. Cap center is always brighter than cap edges, although the entire cap grows dark after $L_s = 93.88$. Cap continues to stay darkened until approximately $L_s = 111$. (b) MAWD water data. Atmospheric water content begins to increase as cap darkens, and peak occurs at approximately $L_s = 111$. In both graphs, average values are plotted with error bars of ± 1 SD.

3.2. Viking IRTM Surface Temperature (T_{20}) Data Results

Viking IRTM T_{20} observations documenting the timing of the retreat and disappearance of the seasonal CO_2 cap and the subsequent exposure and warming of the residual cap and surrounding areas are shown in Figs. 6 and 7. The plots of T_{20} diurnal temperature variations in Fig. 7 indicate that the seasonal CO_2 cap retreated beyond the warm polar sand sea by $L_s = 81$. Consistent with the conclusions of previous studies, the IRTM surface temperature maps of the residual cap area show that the bright ice apparent in the imaging (Part I, Fig. 2) and IRTM albedo data late in the summer season was not carbon dioxide

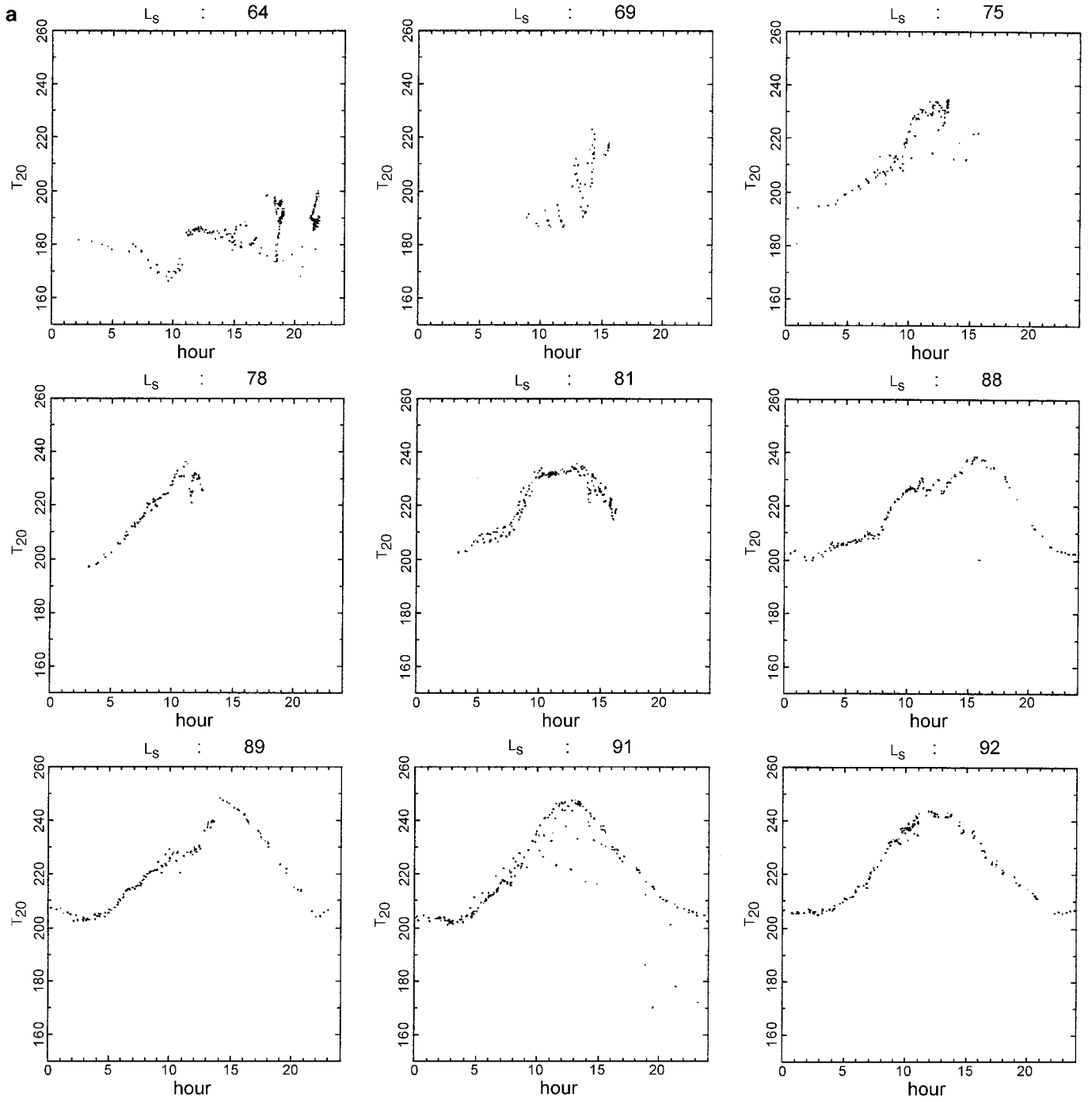

FIG. 7. Diurnal surface temperature variations. (a) Nine diurnal surface temperature variation plots in the latitude range 75–76°N. T_{20} data are plotted for each martian day; days chosen for representation here are indicative of the general trend of the data. Temperatures range from 140 to 260 K. Diurnal cycle is not established until CO_2 cap has retreated beyond 76°N, as shown in plot labeled $L_s = 77.17$. Variation that occurs before the regular diurnal cycle is established is likely due to local topography and/or local ice coverage. (b) Nine diurnal surface temperature variation plots in the latitude range 77–78°N, the region most closely approximating the dark polar sand sea surrounding the cap, which has long been considered the source of atmospheric water vapor. T_{20} data are plotted for each martian day; days chosen for representation here are indicative of the general trend of the data. Temperatures range from 140 to 260 K. Diurnal cycle is not established until CO_2 cap has retreated beyond 78°N, as shown in plot labeled $L_s = 81.55$. Variation that occurs before the regular diurnal cycle is established is likely due to atmospheric effects and partial local ice coverage.

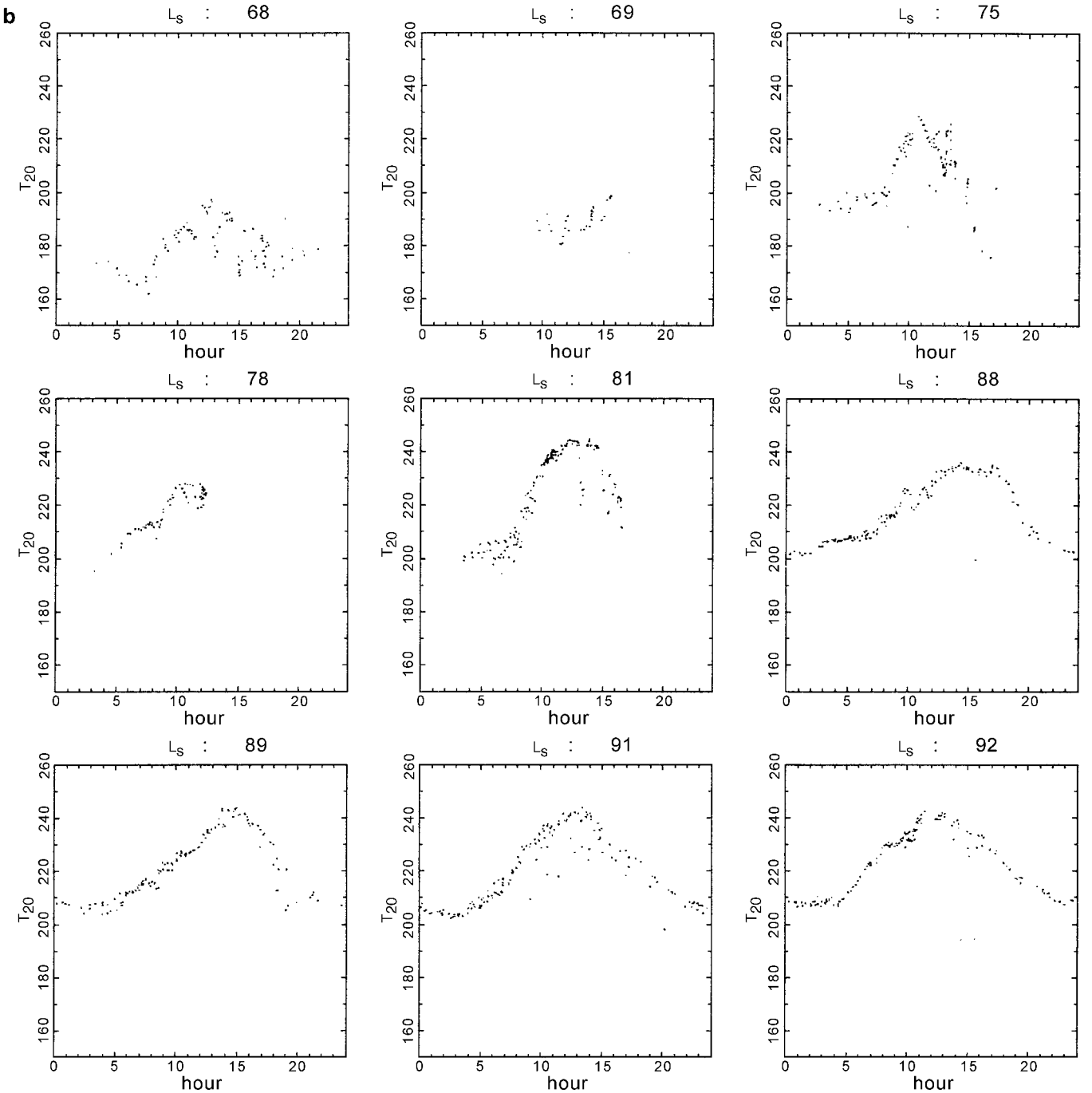

FIG. 7—*Continued*

ice. Surface temperatures were approximately 200 K, which is much higher than the temperature of stable carbon dioxide ice at martian surface pressures (Fig. 8).

3.3. Viking MAWD Data Results

The MAWD north polar water vapor results of this study are generally consistent with those of Davies (1982) and Jakosky and Farmer (1982). We find large-scale agreement with Davies (1982) results; the peak water vapor abundance occurs adjacent to the cap, over the warmer polar sand sea. We also find that the peak water vapor abundance occurs at approximately $L_s = 111$ (Julian date 2443680), consistent with Davies (1982) findings. Jakosky and Farmer (1982) stated that the maximum amount of water vapor was in the atmosphere at $L_s = 120$ (Figs. 1b and 1c). We can not reproduce Jakosky and Farmer (1982) results despite repeated variations of binning both wcp and wvp data.

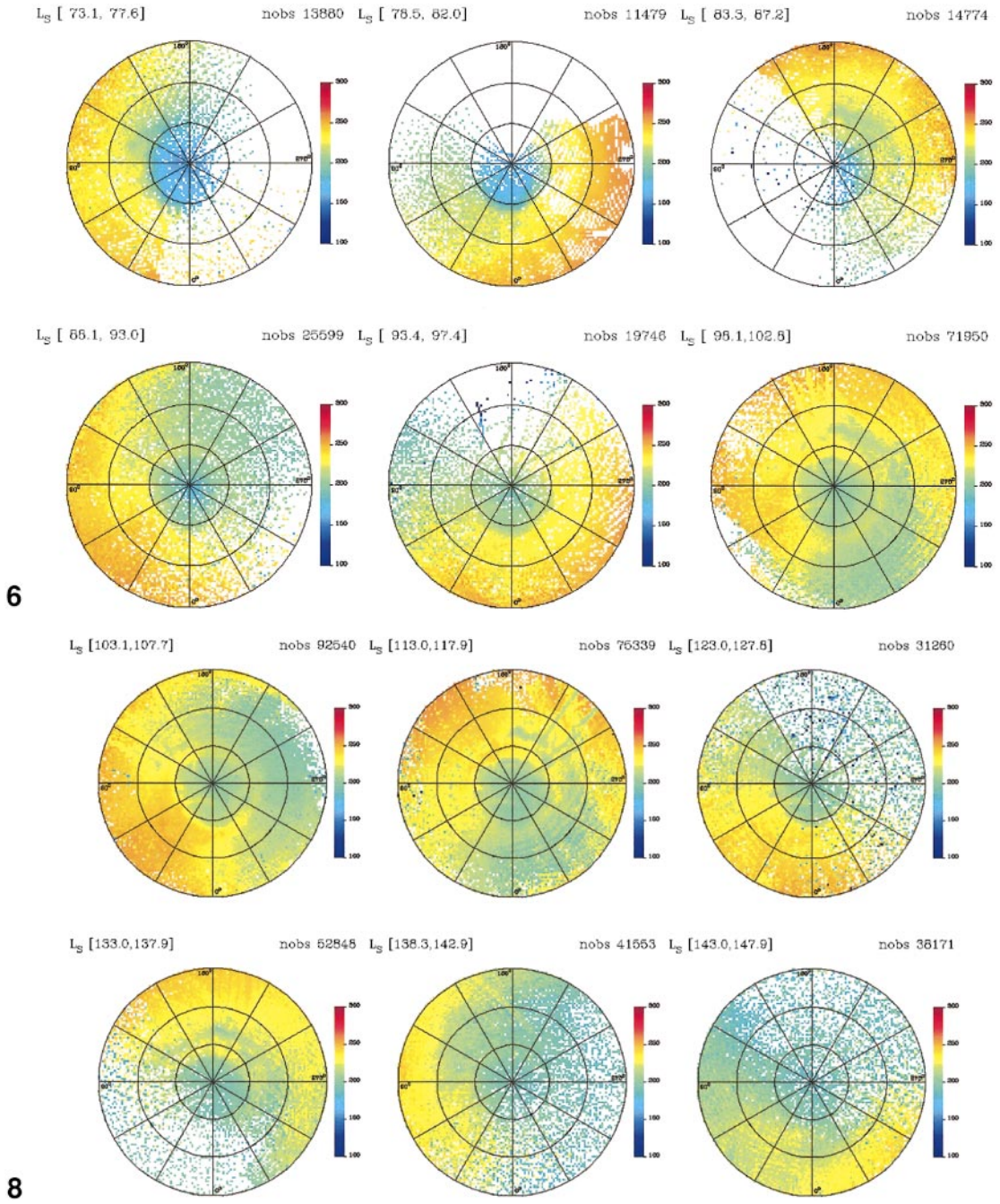

FIG. 6 Six IRTM surface temperature (T_{20} channel) maps of the north polar region of Mars. Maps track final retreat of seasonal CO_2 cap edge by showing increasing temperatures. CO_2 cap has completely disappeared by $L_s = 85.49$ in the fourth map. Maps show data binned in increments of 10 Julian days and those dates are converted to areocentric solar longitude. Nobs refers to the number of observations present in each map. Temperatures range from 100 K (blue) to 300 K (red). Emission angles $<60^\circ$. Twenty-four hours of data are plotted for each day shown.

FIG. 8 Six IRTM T_{20} surface temperature polar maps showing decreasing temperatures as summer season ends. Maps show all data binned in increments of 10 Julian days and those dates are converted to areocentric solar longitude. Each particular map shown was chosen to represent the data closest to the areocentric solar longitudes of the images in Part I, Fig. 2. Nobs refers to the number of observations present in each map. Temperatures range from 100 K (blue) to 300 K (red). Emission angles $<60^\circ$.

The MAWD wcp data used for this study have systematically lower values than the data from Jakosky and Farmer (1982) (Fig. 1b). However, our water abundances closely match those of Davies (1982), as well as matching the timing of the peak atmospheric water vapor amounts from Davies (1982) (Fig. 1c).

3.4. Correlation of Viking IRTM Albedo, T_{20}, and MAWD wcp Data Results

Comparing the time evolution of IRTM albedo, T_{20}, and MAWD wcp data at the north pole (Fig. 9) yields some new insights. The timing of the darkening of the residual cap between $L_s = 70$ and $L_s = 100$ is well correlated with the increase in surface temperatures and atmospheric water vapor content associated with the disappearance of the cold seasonal CO_2 cap. MAWD wcp data indicate that between $L_s = 110$ to $L_s = 180$, atmospheric water vapor decreased at the same time the albedo data showed an increase in cap brightness, while the T_{20} data show a decrease in cap surface temperature. Figure 10 shows Viking IRTM surface temperatures and Viking MAWD atmospheric water data in three different latitude bands in the north polar region as a function of time. The time evolution of water vapor is similar in all three latitude bands whereas surface temperatures increase sooner at lower latitudes than they do at higher latitudes. The largest increase in water vapor of all three regions occurred at $L_s = 90$. Interestingly, at the lower latitude bands, there was no major increase of water vapor in the atmosphere as the carbon dioxide cap sublimed, as would be expected if the vapor moved directly from the surface into the atmosphere. Although some water vapor sublimed when the CO_2 cap sublimed earlier (Fig. 10), the bulk of water is not observed until later. Similarly, at the lower latitude band, water vapor begins decreasing during the summer season well before lower latitude surface temperatures decrease. The best correlation between atmospheric water vapor abundance and temperature is observed at the pole.

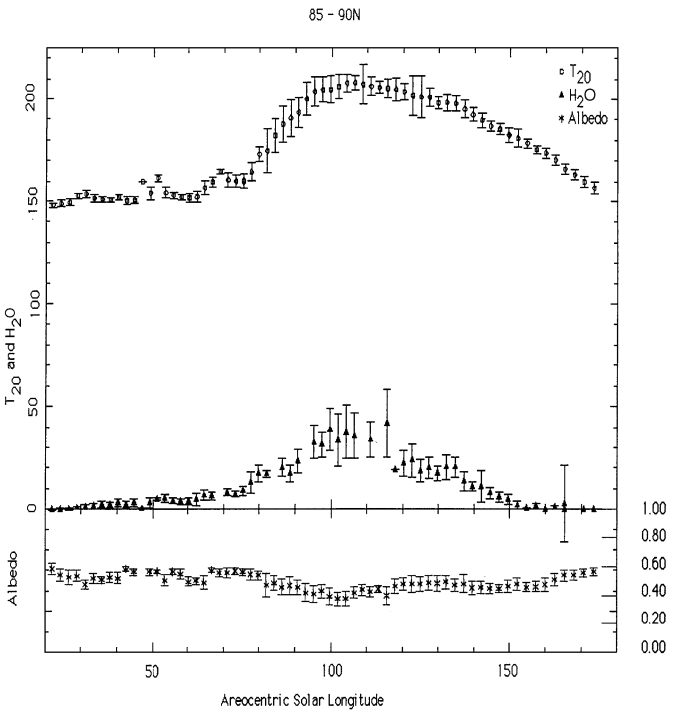

FIG. 9 Viking IRTM T_{20} and albedo data and Viking MAWD atmospheric water vapor data. Zonally averaged IRTM data from latitude 85–90°N were binned in intervals of 5 Julian days and those dates were converted to areocentric solar longitude. The MAWD data were treated similarly. Average values are plotted with error bars of ±1 SD. Vertical axis scales from 0 to 300 K for IRTM T_{20}; the same scale is used to plot MAWD water data, but units are in precipitable micrometers. IRTM albedo data are plotted underneath the two other datasets.

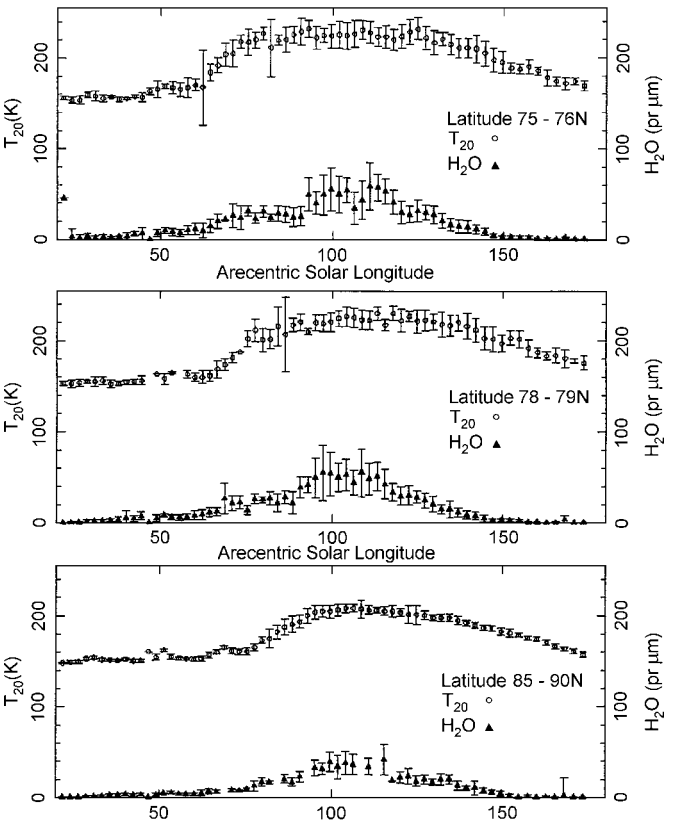

FIG. 10 Viking IRTM T_{20} data and Viking MAWD atmospheric water vapor data. Note the peak of water vapor occurs at the same time in the summer regardless of the latitude. There is no gradual increase of water vapor in the atmosphere as the carbon dioxide cap sublimes (by $L_s = 81.55$) as would be expected if the source of water were directly associated with the regolith. Both datasets were binned in intervals of 5 Julian days and those dates were converted to areocentric solar longitude. Average values are plotted with error bars of ±1 SD. Top graph shows zonally averaged latitude band 75–76°N. Middle graph shows averaged band chosen to cover only the dark polar sand sea—region is 78–79°N, 265–330°W. Bottom graph shows zonally averaged latitude band 85–90°N. Vertical axis scales from 0 to 255 K for IRTM T_{20}; the same scale is used to plot MAWD water data, but units are in precipitable micrometers. When surface temperatures increase beyond 150 K and the residual cap is exposed, some water vapor sublimes into the atmosphere. The dark, thick lines mark the temperature at the cap center greater than 200 K. Shortly after the temperatures increase beyond the nighttime saturation temperature (200 K), atmospheric water vapor increases.

4. DISCUSSION

Viking IRTM data confirm the increase in bright ice coverage on the residual north polar cap during the summer season seen in the imaging data from Part I. Possible explanations for the cap brightening include removal of a layer of dust from the cap exposing an underlying bright layer or deposition of bright ice covering up the darker dust. By showing that the surrounding dark sand does not brighten along with the cap (Fig. 4), we have demonstrated that the effect is not that of cloud coverage later in the season or other atmospheric phenomena that affect the entire region. In the next sections, we discuss these results in light of previous observations and model results.

4.1. Possible Mechanisms Operating in Mars' North Polar Region

A variety of explanations can account for the albedo increase seen in the imaging data (Part I). Possible explanations for the brightening include photometric variation resulting from the spacecraft's changing viewing geometry, illumination variations, atmospheric phenomenon such as clouds, removal of dust from the cap, exposing a brighter underlying surface, and deposition of ice. Ruling out possibilities for the observed brightening in the imaging data is a critical step in determining whether the hypothesis of water deposition on the north polar cap in the summer season is reasonable. Using evidence from Viking IRTM and MAWD data, we demonstrate why the most logical explanation for the brightening of the north polar residual cap in the northern summer is that of deposition of water onto the cap surface late in the summer season.

Comparison of our observations to the results of published models (Haberle and Jakosky 1990, Kieffer 1990, Houben *et al.* 1997) provides an explanation for the brightening visible in the Mariner 9 and Viking imaging datasets. Houben *et al.* (1997) presented a mechanism for moving water vapor poleward as the seasonal CO_2 cap retreats in the spring. In their model, at the edges of the sublimating CO_2 ice cap, water vapor was taken into the atmosphere. Due to baroclinic wave activity at the cap edge, some of this water vapor is transported back across the still iced, colder region at which point the water vapor precipitates out back onto the cap. The regolith and surrounding sand dunes are likely sources for some of the water vapor, but as the water is transported over colder regions it precipitates out and is incorporated into the retreating frozen CO_2 cap. As the season continues, the CO_2 cap gradually decreases in size and continues to move poleward, taking the water ice with it. Finally, just after summer solstice, when the center of the cap reaches the maximum surface temperatures, a large pulse of water vapor is released into the atmosphere, consistent with the MAWD and IRTM observations presented here. Interesting to note is the fact that the maximum amount of atmospheric water vapor occurs over the sand sea (Fig. 10). The Haberle and Jakosky (1990) model indicates that off-cap winds are likely to occur in the north polar region, which would provide a mechanism for moving the water vapor from its final release in the center of the cap to outside the cap over the warmer polar sand sea.

Examination of these models in light of our observations leads us to suggest that it is likely that cold trapping of water produces the brightening regions seen in the northern summer season (Figs. 3 and 10; Part I, Fig. 2). Figure 11 shows a cartoon of the most likely sequence of events in the annual water cycle on Mars. In the fall and winter, the seasonal CO_2 cap covers the bright ice, where it remains until the following spring, when it is possible that the mechanism discussed by Houben *et al.* (1997) moves the water ice to the center of the cap, darkening the appearance of the cap periphery. Off-cap winds (Haberle and Jakosky 1990) may be producing the pulse of water vapor in the polar atmosphere over the sand sea, rather than over the center of the polar cap. Local temperature differentials allow cold trapping of water ice onto the cap surface in the summer, producing the bright cap. Due to decreasing temperatures in the fall season, the seasonal carbon dioxide cap forms again on top of the bright water ice.

4.2. Relation of Models to IRTM Observations

IRTM albedo data show that the cap appeared darkest after $L_s = 93$ (Figs. 3 and 9), which we interpret to indicate that bright water ice has been removed from the bulk of the cap. Additionally, the cap center always remains brighter than the cap edges, which we believe suggests the center is a region of active water ice accumulation and is the local sink for the water vapor for the rest of the cap.

IRTM surface temperature and MAWD atmospheric water vapor data show that although some water vapor sublimated into the atmosphere as the seasonal carbon dioxide cap retreated, the bulk of the water vapor did not enter the atmosphere until the center of the north residual polar cap heated to beyond 200 K at approximately $L_s = 103$. This is the approximate temperature of a surface ice deposit in solid–vapor equilibrium with a well-mixed lower atmosphere containing a total of approximately 50 pr μm of water vapor. Note that the peak of water vapor occurred at the same time in the summer regardless of the latitude (Fig. 10). We suggest the discrepancy in the timing of increasing local atmospheric water vapor may indicate the source for the additional water ice appearing on the cap; on measurable timescales, it does not appear that the water vapor is moving directly into the atmosphere from the regolith or the cap surface. Rather, it appears that the water vapor is moving toward the cap center through its recondensation onto the cap surface along with the retreating carbon dioxide ice. Figure 7 shows that the regular diurnal temperature change was apparent when the minimum diurnal temperature reached a nighttime saturation temperature of $\sim$200 K; it appears that the cap must heat beyond the nighttime saturation temperature for water vapor to be released into the atmosphere. There is a brief time lag between the darkening of the cap at $L_s = 80$ and the appearance of the maximum amount of water vapor in the atmosphere over the residual polar cap at $L_s = 110$ (Fig. 9). The time lag indicates

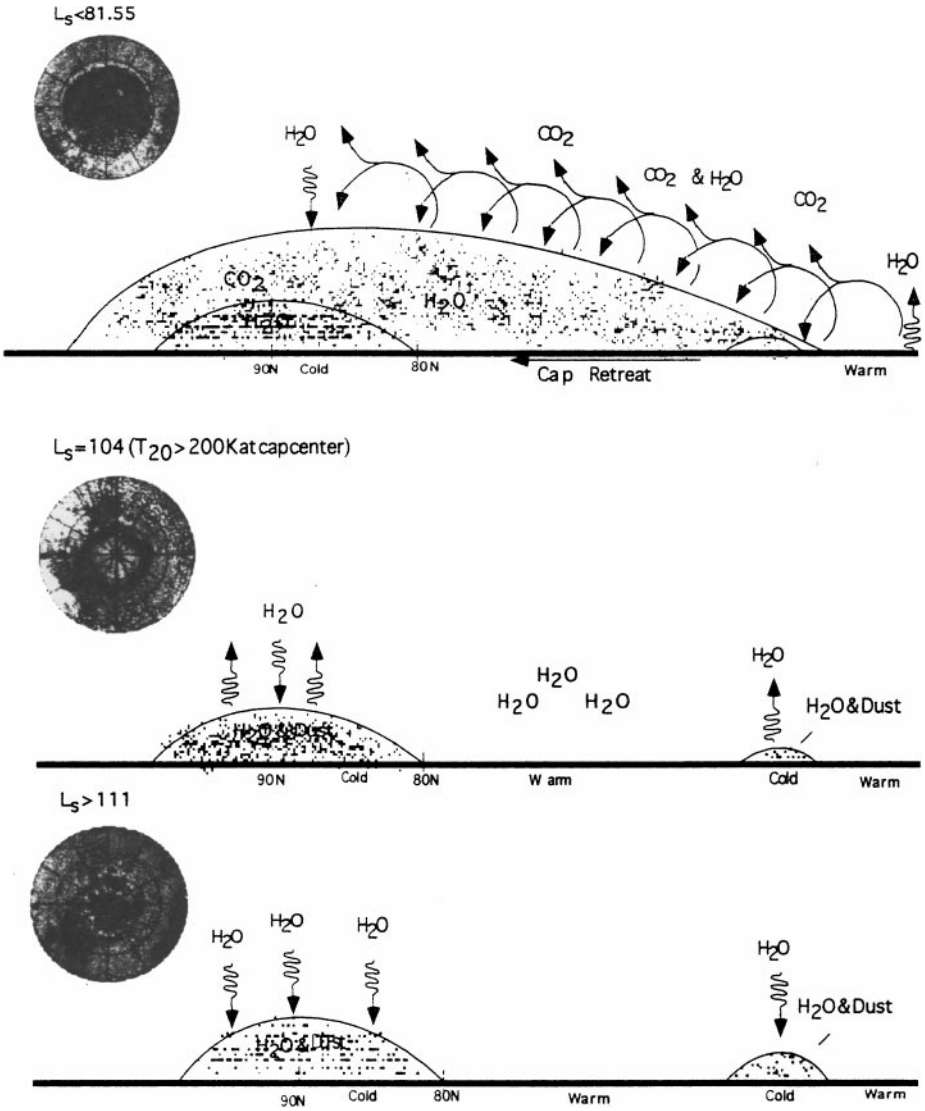

FIG. 11. Cartoon of mechanisms possibly involved in cycling water on Mars. First panel shows what is occurring in the springtime, while the CO_2 cap is retreating. Water vapor is "vacuumed" up along with retreating carbon dioxide and deposited onto the cap. Inset shows albedo of cap before $L_s = 81.55$. Second panel shows conditions when the surface temperatures reach 200 K. Cap and outliers are at their minimum extent. Note continued anomalous bright cap center, potentially indicating a cold trap and active water deposition. Third panel shows increasing brightening of cap and associated outliers due to cold trapping of ice on areas that always have more ice or ground ice relative to the bare, darker and warmer ground. Insets show brightening of cap and layered terrains later in the summer.

that local temperature differences govern some fraction of the water transport in the north polar region; some water is released into the atmosphere as the surface heats up. This contradicts lower resolution studies that indicated that the *direct* source of water vapor seen in the MAWD data was the regolith surrounding the cap (e.g., Houben *et al.* 1997, Jakosky and Farmer 1982). We suggest instead that the primary global source of water is the retreating seasonal cap itself, as well as any additional water vapor incorporated into the cap from the surrounding regolith and sand dunes.

As surface temperatures in the northern hemisphere decreased later in the summer, water vapor could no longer be held in the atmosphere and condensed back onto the cap (Fig. 10). Late summer condensation of water vapor is consistent with the brightening visible in the imaging data (Part I, Fig. 2), and MAWD data do indeed show that, at the same time the cap brightened in the imaging and IRTM albedo data (Part I, Fig. 1a), atmospheric water vapor decreased. MAWD data also indicate there was some transport of water vapor away from the northern polar region in the early summer toward the equator (Haberle and Jakosky, 1990). However, it appears that the bulk of the atmospheric water vapor remained in the northern polar region after its release from the seasonal cap and/or the regolith.

In the scenario we have just outlined, the seasonal cycle of surface water is as follows: The north polar region is covered with CO_2 all winter long. In the spring, after the CO_2 cap retreats, a thin layer of water ice moves toward the cap center where it accumulates between $L_s = 93$ and $L_s = 103$, resulting in the bright-centered and dark-edged cap seen in observations (e.g., Part I, Fig. 1a). After $L_s = 103$, water vapor is released from the cap center into the atmosphere. When the nighttime saturation temperature reaches 200 K, the thin layer of water ice is gradually deposited onto the cap from $L_s \approx 111$–140, before the seasonal carbon dioxide cap returns in the fall (Fig. 11).

4.3. Viking IRTM Thermal Inertia Maps

Paige *et al.* (1994) mapped the apparent thermal inertia and albedo of the north polar region of Mars. These maps have significance in that the regions that are shown to brighten during the summer season in this study have high thermal inertias, and regions that do not brighten have lower thermal inertias. This is consistent with our conclusion that cold trapping is the most likely mechanism for brightening. It is also consistent with the notion that accumulation is occurring in areas of high thermal inertia. Paige *et al.* (1994) also interpreted the high thermal inertia measurements to indicate the presence of dense, coarse-grained or solid ice that extends from close to the surface downward at least 10 cm.

In the thermal inertia maps, the cap center at 90°N, 250–270°W has a lower thermal inertia than the surrounding portions of the cap. A lower thermal inertia indicates smaller or less annealed ice grains, which is consistent with the interpretation of younger, accumulating ice at the cap center.

5. CONCLUSIONS

The IRTM and MAWD observations presented here show:

1. The residual cap had the lowest albedo between $L_s = 93$ and $L_s = 103$.
2. Water vapor was not released into atmosphere until the surface temperatures at the cap center reached their maximum at $L_s = 103$.
3. The albedo of the residual polar cap increased later in the summer season.
4. Surface temperatures during the summer season were not consistent with recondensation of CO_2 frost on the cap surface.
5. The cap center remained brighter than the rest of the cap at all seasons.
6. Regions that increased in brightness during the summer season correlate with regions that had high thermal inertia.

5.1. Implications for Seasonal Cycles

Cold trapping is the most likely mechanism to explain the appearance of bright ice in the late summer. In Paper I, we suggested that the late summer cap albedo increase could have been produced by a minimum of tens of precipitable micrometer of ice and dust deposited on the surface. MAWD water data indicate that the martian atmosphere held an average of 10 pr μm. Therefore, it is plausible that the water vapor observed in the atmosphere in the MAWD data condensed as surface temperatures decreased in the summer season. We believe our quantitative work on estimating deposition could provide constraints on models for the rate of potential accumulation under present conditions.

Haberle and Jakosky (1990) note that the rate of water vapor rising in the atmosphere of the southern hemisphere is less than the rate of falling atmospheric water vapor concentration in the northern hemisphere. They suggest that there must be additional sinks for water vapor, and it may be that some water vapor does not cross the equator but rather may be deposited on the northern residual polar cap. In support of this conclusion, Haberle and Jakosky (1990) pointed out that the high-latitude summertime circulation lacks the strength to move water vapor to lower latitudes, likely due to the lower elevations in the northern hemisphere. This is consistent with the notion that water vapor is redeposited in the northern hemisphere. However, because the total amount of water vapor that we believe is involved in the summertime residual cap albedo variations is quite small, it is not likely to be significant on a hemispheric scale.

5.2. Implications for Long-Term Climate Change

Although water is lost from the northern hemisphere (Haberle and Jakosky 1990), there are several lines of evidence that the water cycle tends toward closure in the vicinity of the polar cap. First, IRTM and MAWD data showed that the amount of atmospheric water vapor did not increase until the center of the cap reached its maximum surface temperature. IRTM, MAWD, and imaging data showed that water vapor appears to have been redeposited on the cap. Second, there was no interannual variation of this cycle in the years that data were acquired. These observations tend to close the water cycle in the vicinity of the polar cap.

It is difficult to extrapolate these results to those relating to long-term climate change because we do not have an extended record. However, our results suggest that active seasonal processes have macroscopic effects that are observable from orbit. Further, albedo data suggest that the cap center has somewhat different characteristics than the cap edge. Although there is no definitive evidence regarding ice flow in the northern hemisphere of Mars, Mars Orbiter Laser Altimeter data indicate that the cap center is the highest portion of the cap (Zuber *et al.* 1998). Therefore, if any regions are accumulating annual layers, the cap center is the most likely location. We also point out that the cap center has a favorable energy balance with respect to accumulation due to the increased brightness. Finally, the timing of this study is fortunate as many of these conclusions could be tested by missions to Mars in coming years.

ACKNOWLEDGMENTS

We thank Bruce Jakosky and Howard Houben for reviews of an earlier version of the manuscript. This research was supported by the National Aeronautics and Space Administration under Grant NAGW 4327 and by the NASA Graduate Student Researchers Program, NGT- 51273. We owe special thanks to Robert Mehlman for allowing us access to his tape archive containing the Viking Orbiter MAWD data. Thanks also to Richard Zurek for his invaluable insight into the original processing of the MAWD data.

REFERENCES

Bass, D. S., K. E. Herkenhoff, and D. A. Paige 2000. Variability of Mars' north polar water ice cap. I. Analysis of Mariner 9 and Viking Orbiter imaging data. *Icarus* **144**, 382–396.

Davies, D. W. 1982. Water vapor in Mars' arctic: Seasonal and spatial variability. *J. Geophys. Res.* **87**, 10,253–10,263.

Davies, D. W., C. B. Farmer, and D. D. La Porte 1977. Behavior of volatiles in Mars' polar areas: A model incorporating new experimental data. *J. Geophys. Res.* **82**, 3815–3822.

Fanale, F. P., S. E. Postawko, J. B. Pollack, M. H. Carr, and R. O. Pepin 1992. Mars: Epochal climate change and volatile history. In *Mars* (H. H. Kieffer, B. M. Jakosky, C. W. Snyder, and M. S. Matthews, Eds.), pp. 1135–1179. Univ. of Arizona Press, Tucson.

Farmer, C. B., D. W. Davies, and D. D. La Porte 1976. Mars' northern summer ice cap: Water vapor observations from Viking 2. *Science* **194**, 1339–1341.

Haberle, R. M., and B. M. Jakosky 1990. Sublimation and transport of water from the north residual polar cap of Mars. *J. Geophys. Res.* **95**, 1423–1437.

Houben, H., R. M. Haberle, R. E. Young, and A. Zent 1997. Modeling the martian seasonal water cycle. *J. Geophys Res.* **102**, 9069–9083.

Howard, A. D., J. A. Cutts, and K. J. Blasius 1982. Stratigraphic relationships within the martian polar cap deposits. *Icarus* **50**, 161–215.

Jakosky, B. M., and C. B. Farmer 1982. The seasonal and global behavior of water vapor in the Mars atmosphere: Complete global results of the Viking Atmospheric Water Detector Experiment. *J. Geophys. Res.* **87**, 2999–3019.

Jakosky, B. M., and R. M. Haberle 1992. The seasonal behavior of water on Mars. In *Mars* (H. H. Kieffer, B. M. Jakosky, C. W. Snyder, and M. S. Matthews, Eds.), pp. 969–1016. Univ. of Arizona Press, Tucson.

Jouzel, J., C. Lorius, J. R. Petit, C. Genthon, N. I. Markov, V. M. Kotlyakov, and V. M. Petrov 1987. Vostok ice core: A continuous isotope temperature record over the last climatic cycle (160,000 years). *Nature* **329**, 403–408.

Kieffer, H. H., S. C. Chase, Jr., T. Z. Martin, E. D. Miner, and F. D. Palluconi 1976. Martian north pole summer temperatures: Dirty water ice. *Science* **194**, 1341–1344.

Kieffer, H. H., T. Z. Martin, A. R. Peterfreund, B. M. Jakosky, E. D. Miner, and F. D. Palluconi 1977. Thermal and albedo mapping of Mars during the Viking primary mission. *J. Geophys. Res.* **82**, 4249–4291.

Kahn, R. A., T. Z. Martin, R. W. Zurek, and S. W. Lee 1992. The martian dust cycle. In Mars (H. H. Kieffer, B. M. Jakosky, C. W. Snyder, and M. S. Matthews, Eds.), pp. 1017–1053. Univ. of Arizona Press, Tucson.

Paige, D. A., and A. P. Ingersoll 1985. Annual heat balance of martian polar caps-Viking observations. *Science* **228**, 1160–1168.

Paige, D. A., J. E. Bachman, and K. E. Keegan 1994. Thermal and albedo mapping of the polar regions of Mars using Viking thermal mapper observations. 1. North polar region. *J. Geophys. Res.* **99**, 25,959–25,991.

Snyder, C. W. 1979. The planet Mars as seen at the end of the Viking mission. *J. Geophys. Res.* **84**, 8487–8519.

Zuber, M. T., D. E. Smith, S. C. Solomon, J. B. Abshire, R. S. Afzal, O. Ahronson, K. Fishbaugh, P. G. Ford, H. V. Frey, J. B. Garvin, J. W. Head, A. B. Ivanov, C. L. Johnson, D. O. Muhleman, G. A. Neumann, G. H. Pettengill, R. J. Phillips, X. Sun, H. J. Zwally, W. B. Banerdt, and T. C. Duxbury 1998. Observations of the north polar region of Mars from the Mars Orbiter Laser Altimeter. *Science* **282**, 2053–2060.

Zurek, R. W., and L. J. Martin 1993. Interannual variability of planet-encircling dust storms on Mars. *J. Geophys. Res.* **98**, 3247–3260.